



AALBORG UNIVERSITY
DENMARK

Aalborg Universitet

An active damper for stabilizing power-electronics-based AC systems

Wang, Xiongfei; Blaabjerg, Frede; Liserre, Marco; Chen, Zhe; He, Jinwei; Li, Yunwei

Published in:
I E E E Transactions on Power Electronics

DOI (link to publication from Publisher):
[10.1109/TPEL.2013.2278716](https://doi.org/10.1109/TPEL.2013.2278716)

Publication date:
2014

Document Version
Early version, also known as pre-print

[Link to publication from Aalborg University](#)

Citation for published version (APA):
Wang, X., Blaabjerg, F., Liserre, M., Chen, Z., He, J., & Li, Y. (2014). An active damper for stabilizing power-electronics-based AC systems. *I E E E Transactions on Power Electronics*, 29(7), 3318-3329.
<https://doi.org/10.1109/TPEL.2013.2278716>

General rights

Copyright and moral rights for the publications made accessible in the public portal are retained by the authors and/or other copyright owners and it is a condition of accessing publications that users recognise and abide by the legal requirements associated with these rights.

- Users may download and print one copy of any publication from the public portal for the purpose of private study or research.
- You may not further distribute the material or use it for any profit-making activity or commercial gain
- You may freely distribute the URL identifying the publication in the public portal -

Take down policy

If you believe that this document breaches copyright please contact us at vbn@aub.aau.dk providing details, and we will remove access to the work immediately and investigate your claim.

© 2013 IEEE. Personal use of this material is permitted. Permission from IEEE must be obtained for all other uses, in any current or future media, including reprinting/republishing this material for advertising or promotional purposes, creating new collective works, for resale or redistribution to servers or lists, or reuse of any copyrighted component of this work in other works.

Digital Object Identifier (DOI): [10.1109/TPEL.2013.2278716](https://doi.org/10.1109/TPEL.2013.2278716)

IEEE Transactions on Power Electronics, Vol. PP, No. 99, Early Access Article, Aug. 2013.

An Active Damper for Stabilizing Power Electronics Based AC Systems

Xiongfei Wang
Frede Blaabjerg
Marco Liserre
Zhe Chen
Jinwei He
Yunwei Li

Suggested Citation

X. Wang, F. Blaabjerg, M. Liserre, Z. Chen, J. He, and Y. Li, "An active damper for stabilizing power electronics based AC systems," *IEEE Trans. Power Electron.*, vol. PP, no. 99, Early Access Article, Aug. 2013.

An Active Damper for Stabilizing Power Electronics Based AC Systems

Xiongfei Wang, *Member, IEEE*, Frede Blaabjerg, *Fellow, IEEE*, Marco Liserre, *Fellow, IEEE*, Zhe Chen, *Senior Member, IEEE*, Jinwei He, *Student Member, IEEE*, and Yunwei Li, *Senior Member, IEEE*

Abstract—The mutual interactions in the parallel grid-connected converters coupled through the grid impedance tend to result in a number of stability and power quality problems. To address them, this paper proposes an active damper based on a power converter with the high control bandwidth. The general idea behind this proposal is to dynamically reshape the grid impedance profile seen from the point of common coupling of the converters, such that the potential oscillations and resonance propagation in the parallel grid-connected converters can be mitigated. Further, to validate the effectiveness of the active damper, simulations and experimental tests on a three-converter based setup are carried out. The results show that the active damper can become a promising way to stabilize the power electronics based AC power systems.

Index Terms—Grid-connected converters, grid impedance, paralleled operation, stability, resonance propagation

I. INTRODUCTION

Over the last years, the power electronics converters are gaining a wide acceptance as a flexible and efficient grid interface for connecting renewable energy systems and at the load side as electric drives [1], [2]. The mutual interactions between the control loops of the parallel grid-connected converters coupled via the grid impedance, such as the wind turbines converters in wind farms [3], the Photovoltaic (PV) inverters in PV power plants [4], and the locomotive converters in the electric railway networks [5], will be inevitable, which may result in the undesired small-signal oscillations. Further, due to the popular use of *LCL*-filters, the additional resonances may arise in the paralleled converters and vary with the different number of converters. This fact in turn reduces the allowed control bandwidth of converters, and in some cases brings in the under-damped resonances [6]-[8].

Manuscript received January 29, 2013; revised April 26, 2013; July 03, 2013; accepted August 08, 2013. This work was supported by European Research Council under the European Union's Seventh Framework Program (FP/2007-2013)/ERC Grant Agreement n. [321149-Harmony].

X. Wang, F. Blaabjerg, M. Liserre, and Z. Chen are with the Department of Energy Technology, Aalborg University, 9220 Aalborg East, Denmark (e-mail: xwa@et.aau.dk; fbl@et.aau.dk; mli@et.aau.dk; zch@et.aau.dk).

J. He and Y. Li are with the Department of Electrical and Computer Engineering, University of Alberta, Edmonton, AB T6G 2R3, Canada (e-mail: hjinwei@ualberta.ca; yunwei.li@ualberta.ca)

There is, consequently, an urgent need to develop effective measures to address the aforementioned challenges. In [9], the impedance-based stability analysis approach, originating from the Middlebrook's Extra Element Theorem [10], provides a powerful tool to gain the insight of the interactions in the paralleled converters. It has been shown that a non-negative real part of the input admittance of a grid-connected converter is usually required for damping oscillations [11]-[13]. Hence, to dampen out the resonance propagation in the parallel grid-connected PV inverters with *LCL*-filters, the Resistive-Active Power Filter (R-APF) method is implemented in [14], where the inverters are controlled to behave as resistive loads at the non-fundamental frequencies. However, in this case, a high-bandwidth current controller is needed in order to cover a wide range of resonant frequencies, which poses a challenge for the converters with the low ratio of sampling-to-fundamental frequencies. Further, the performance of the R-APF method is affected by the grid-side inductances in the *LCL*-filters [15]. As opposite to synthesizing a resistive load, a filter-based approach is reported in [3], where a wideband notch filter is inserted into the current control loop of the wind turbine converters, such that the resonances in a wind power plant can be dampened out. The main problem in this method is that the notch filter design is highly dependent on the system conditions, and thus its stabilizing performance may be degraded under the system parameter variations [16].

In this work, instead of reshaping the input admittances of the grid-connected converters with the different control loops, an active damper based on a power converter with the high control bandwidth is proposed. The active damper is installed at the Point of Common Coupling (PCC) of the paralleled converters, and is controlled to be a variable resistance at the frequencies where the resonance arises. Thus, the grid impedance seen from the PCC can be dynamically adjusted by the active damper, and the resonances resulting from the interactions in the parallel grid-connected converters can effectively be mitigated.

This paper presents first a small-signal stability analysis of a power electronics based AC system including two paralleled active rectifiers with the *LCL*-filters in Section II. The mutual interactions between the current control loops of the rectifiers as well as the effect of the grid impedance variation are assessed by the Nyquist stability criterion. Then, in light of the

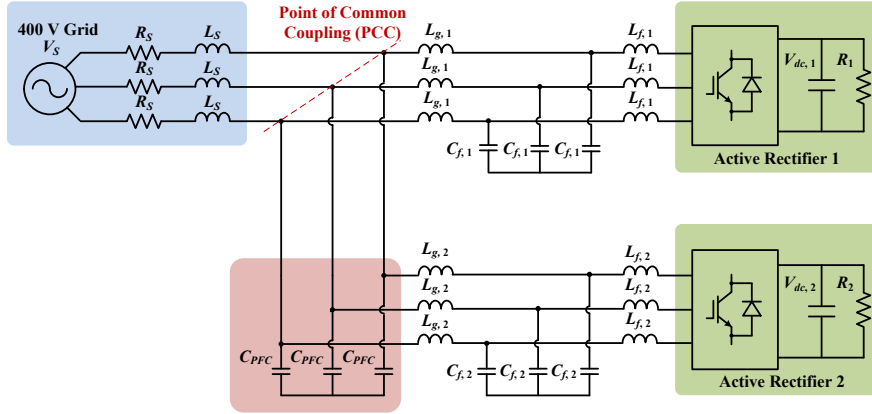


Fig. 1. A balanced three-phase power electronics based AC system with two paralleled active rectifiers.

analysis results, the operation principle of the proposed active damper is discussed in Section III, including the basic configuration and the control schemes. This is followed by an assessment on the stabilizing effect of the active damper in the frequency domain. Finally, in Section IV, to further validate the performance of the active damper, the time domain simulations and experiments on a three-converter based setup are performed. The results show that the proposed active damper concept provides a flexible way to address the stability and power quality problems in the power electronics based AC systems.

II. STABILITY ANALYSIS OF PARALLEL GRID-CONNECTED CONVERTERS WITH *LCL*-FILTERS

A. System Description

Fig. 1 illustrates a balanced three-phase power electronics based AC system, where two active rectifiers are connected to the PCC, and a Power Factor Correction (PFC) capacitor C_{PFC} is installed at the PCC. In such a system, the small-signal oscillations can arise in the different ways. A straightforward way is the unstable control loop of the active rectifier when connecting it to a stiff AC grid with nearly zero grid impedance [17]. The second case is that the input admittance of active rectifier may exhibit the negative real part at the low frequencies depending on the dynamics of the outer DC-link voltage and reactive power control loops as well as the Phase Locked-Loop (PLL). As a consequence, the low frequency oscillations may be triggered even with a single active rectifier [11]-[13], [18]. The third case is due to the system impedance variation at the PCC of active rectifiers, which can result from the change of grid impedance [19], and the input admittance of the other paralleled rectifiers [14].

In this work, the active rectifiers are designed with a stable behavior seen from the PCC. The dynamics of the outer power control and synchronization loops are designed much slower than the inner current control loop. Thus, the low frequency oscillations caused by the outer control loops can be neglected for the sake of simplicity. Consequently, only the third case is

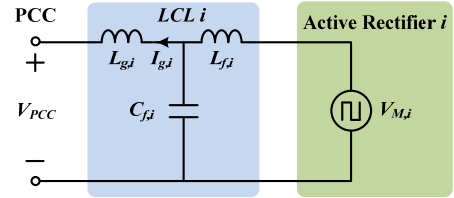


Fig. 2. Simplified circuit for the i -th ($i=1, 2$) active rectifier.

concerned, which implies that the mutual interactions between the current control loops of the paralleled rectifiers can be characterized by their closed-loop input admittances [11]. The impedance-based stability analysis method, which is based on the terminal behavioral models of rectifiers, can thus be used to identify the nature of their mutual interactions [20]-[23].

B. Modeling of Parallel Grid-Connected Converters

Fig. 2 depicts the simplified circuit for the i -th ($i=1, 2$) active rectifier, where the voltage source converter is represented by the modulated voltage source $V_{M,i}$, and the grid-side current is controlled for a better stability of the control system [24]. Thus, the frequency behavior of the *LCL*-filter seen from the PCC can be expressed by the following two admittances

$$Y_{M,i} = \left. \frac{I_{g,i}}{V_{M,i}} \right|_{V_{PCC}=0} = \frac{Z_{Cf,i}}{Z_{Cf,i}Z_{Lf,i} + Z_{Lg,i}Z_{Lf,i} + Z_{Cf,i}Z_{Lg,i}} \quad (1)$$

$$Y_{o,i} = \left. \frac{-I_{g,i}}{V_{PCC}} \right|_{V_{M,i}=0} = \frac{Z_{Lf,i} + Z_{Cf,i}}{Z_{Cf,i}Z_{Lf,i} + Z_{Lg,i}Z_{Lf,i} + Z_{Cf,i}Z_{Lg,i}} \quad (2)$$

where $Z_{Lf,i}$, $Z_{Cf,i}$ and $Z_{Lg,i}$ are the impedances for the inductor $L_{f,i}$, the capacitor $C_{f,i}$, and the inductor $L_{g,i}$, respectively.

Fig. 3 depicts the block diagram of the grid-side current control loop for the i -th active rectifier, where the Proportional plus Resonant (PR) current controller is used in the stationary $\alpha\beta$ -frame [25]. From Fig. 3, the Norton equivalent circuit of

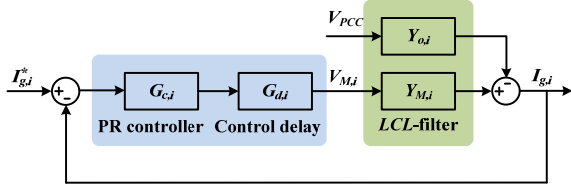


Fig. 3. Block diagram of the current control loop for the i -th active rectifier.

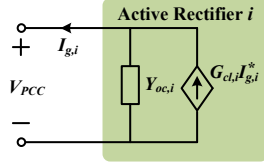


Fig. 4. The Norton equivalent circuit for the i -th active rectifier with the closed current control loop.

the i -th active rectifier with the current control loop closed can be derived, which is shown in Fig. 4. Thus, the terminal behavioral model of the i -th active rectifier seen from the PCC can be derived as

$$I_{g,i} = G_{cl,i} I_{g,i}^* - Y_{oc,i} V_{PCC} \quad (3)$$

$$G_{cl,i} = \frac{T_{c,i}}{1 + T_{c,i}}, \quad Y_{oc,i} = \frac{Y_{o,i}}{1 + T_{c,i}} \quad (4)$$

where $I_{g,i}^*$ is the current reference for the i -th active rectifier, $G_{cl,i}$ is the closed-loop gain of the current control loop, and $Y_{oc,i}$ is the closed-loop input admittance. $T_{c,i}$ is the open-loop gain of the current control loop, which is derived as

$$T_{c,i} = G_{c,i} G_{d,i} Y_{M,i} \quad (5)$$

where $G_{c,i}$ is the PR current controller and $G_{d,i}$ is the approximated 1.5 sampling period ($T_{s,i}$) delay in the digital control [26], which are expressed as

$$G_{c,i} = K_{pc,i} + \frac{K_{ic,i} s}{s^2 + \omega_f^2} \quad (6)$$

$$G_{d,i} = e^{-1.5T_{s,i}s} \approx \frac{1 - 1.5T_{s,i}s/2 + (1.5T_{s,i}s/12)^2}{1 + 1.5T_{s,i}s/2 + (1.5T_{s,i}s/12)^2} \quad (7)$$

where ω_f denotes the fundamental frequency of the AC system.

Fig. 5 illustrates the closed-loop model of the power electronics based AC system shown in Fig. 1 by substituting the active rectifiers with the Norton equivalent circuits. Y_C is the admittance of the PFC capacitor C_{PFC} , Z_S is the grid impedance including L_S and R_S . It is clear that there are three

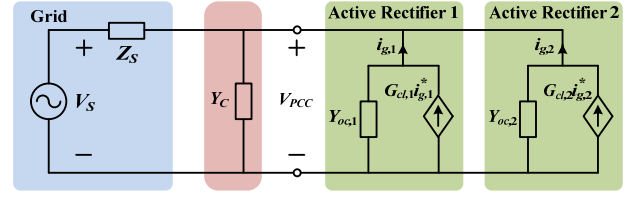


Fig. 5. Closed-loop model of the power electronics based AC system.

closed-loop gains for characterizing the response of the grid-side current in the i -th active rectifier, which are expressed as

$$I_{g,i} = \frac{1}{1 + T_{m,i}} G_{cl,i} I_{g,i}^* - \frac{T_{m,i}}{1 + T_{m,i}} G_{cl,j} I_{g,j}^* - \frac{T_{m,i}}{1 + T_{m,i}} \left(\frac{V_S}{Z_S} \right) \quad (8)$$

where the term ' j ' denotes the other active rectifier ($i \neq j$). $T_{m,i}$ is the gain of the so-called minor feedback loop, which describes the loading effect of the system impedance at the PCC of active rectifiers, and can be expressed as

$$T_{m,i} = \frac{Y_{oc,i}}{Y_{to,i}}, \quad Y_{to,i} = \frac{1}{Z_S} + Y_C + Y_{oc,j} \quad (9)$$

where $Y_{to,i}$ is the system admittance seen by the i -th active rectifier at the PCC, which consists of the closed-loop input admittance of the other j -th rectifier, the grid admittance, and the admittance of the PFC capacitor.

C. Impedance-Based Stability Analysis

Table I summarizes the electrical constants for the power electronics based AC system. The main controller parameters of the active rectifiers are listed in Table II. On the basis of these parameters, the frequency response of the open-loop gain of the current control loop $T_{c,i}$ is plotted in Fig. 6, where a stable terminal behavior of the active rectifier seen from the PCC can be observed. This implies that the closed-loop gains of the active rectifiers $G_{cl,i}$ and $G_{cl,j}$ have no poles in the right-half plane, and thus providing a theoretical basis for employing the impedance-based stability criterion [9], [20]-[23]. Then, the stability of the whole system can be assessed through the frequency domain response of the minor-loop gain derived in (9).

To clearly see the effect of the dynamic interactions between the paralleled active rectifiers, the single active rectifier operation case is first evaluated with the different grid inductance. Then, the paralleled operation of active rectifiers is assessed by considering the effect of the input admittance of the other j -th rectifier.

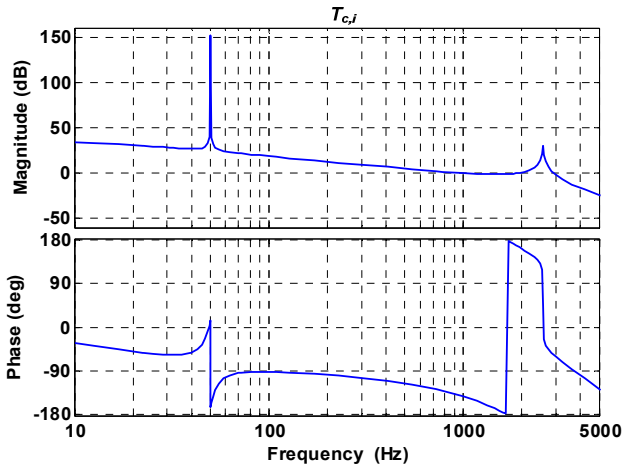
Fig. 7 compares the Nyquist plots for the minor-loop gains $T_{m,i}$ of single active rectifier with the different grid inductances. Notice that the minor-loop gain has no poles in the right-half plane due to the stable terminal behavior of the active rectifiers at the PCC. The number of encirclements of the point $(-1, j0)$ indicates the number of unstable closed-loop

TABLE I. SYSTEM ELECTRICAL CONSTANTS

Electrical Parameters		Values
Grid impedance (Z_S)	L_S	1.2 mH
	R_S	0.4 Ω
PFC capacitor	C_{PFC}	20 μF
LCL-filters	$L_{f,1} = L_{f,2}$	1.5 mH
	$R_{L_{f,1}} = R_{L_{f,2}}$	0.1 Ω
	$C_{f,1} = C_{f,2}$	4.7 μF
	$R_{C_{f,1}} = R_{C_{f,2}}$	0.068 Ω
	$L_{g,1} = L_{g,2}$	1.8 mH
	$R_{L_{g,1}} = R_{L_{g,2}}$	0.2 Ω
DC-link voltages	$V_{dc,1} = V_{dc,2}$	700 V
DC loads	$R_1 = R_2$	400 Ω

TABLE II. MAIN CONTROLLER PARAMETERS OF ACTIVE RECTIFIERS

Controller Parameters		Values
Switching frequency	f_{sw}	10 kHz
Sampling period	T_S	100 μs
PR current controller	$K_{pc,1} = K_{pc,2}$	18
	$K_{ic,1} = K_{ic,2}$	900
Harmonic resonant current controller	$K_{i5,1} = K_{i5,2}$	600
	$K_{i7,1} = K_{i7,2}$	600
	$K_{i11,1} = K_{i11,2}$	600
	$K_{i13,1} = K_{i13,2}$	600
DC-link voltage controller	$K_{p,dc1} = K_{p,dc2}$	0.05
	$K_{i,dc1} = K_{i,dc2}$	0.5


 Fig. 6. Frequency response for the open-loop gain of the current control loop in the i -th rectifier.

poles of the whole system. It is seen that the active rectifier becomes unstable when the grid inductance L_S is equal to 0.6 mH, which indicates that the grid impedance variation has an important effect on the stability of active rectifier [19].

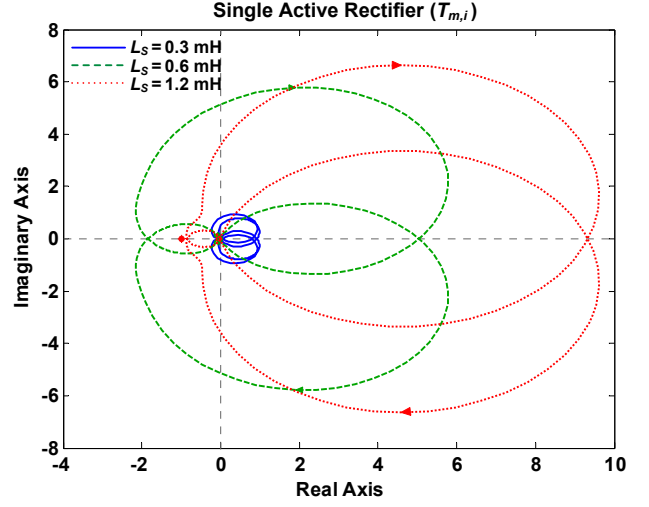


Fig. 7. Nyquist plots of the minor-loop gains derived with the different grid inductance in the case of single active rectifier.

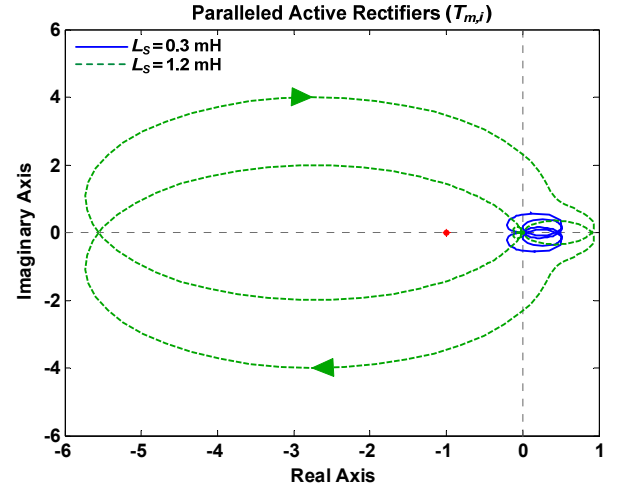


Fig. 8. Nyquist plots of the minor-loop gains derived with the effect of the input admittance of the other paralleled active rectifier.

Fig. 8 shows the Nyquist plots of the minor-loop gain for the paralleled operation of active rectifiers. Since in the case of L_S equal to 0.6 mH, the current control loop is already unstable for the single active rectifier, this is not considered in Fig. 8. However, it is interesting to note that the current control loop becomes unstable when L_S is equal to 1.2 mH, rather than being marginally stable as shown in Fig. 7. To further identify the resonance frequency in this unstable case, the closed-loop response of the minor feedback loop, $T_{m,i}/(1+T_{m,i})$ is depicted in Fig. 9, where the resonances arising around the 35th harmonic can be observed.

Further, it is also important to note that such impedance interactions of the paralleled converters may result in unstable oscillations when multiple harmonic controllers are employed. This is demonstrated in the following by using the 5th, 7th, 11th, and 13th harmonic controllers:

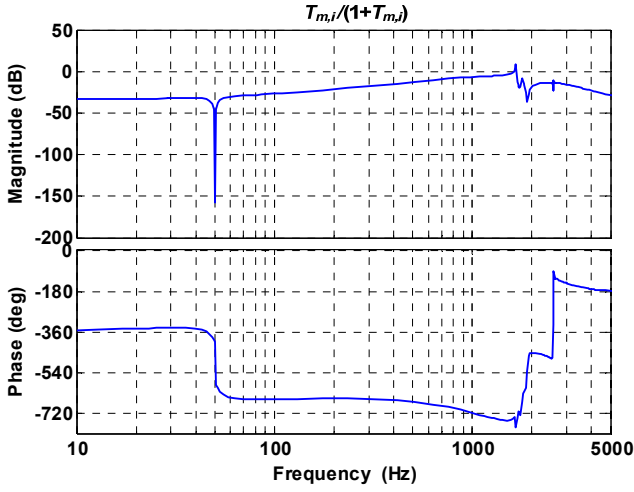


Fig. 9. Frequency response of the closed-loop gain of the minor feedback loop in the resonant case ($L_S = 1.2$ mH).

$$G_{c,i} = K_{pc,i} + \frac{K_{ic,i}s}{s^2 + \omega_f^2} + \sum_{h=5,7,11,13} \frac{K_{ih,i}s}{s^2 + (h\omega_f)^2} \quad (10)$$

where $K_{ih,i}$ denotes the gains of the harmonic resonant controllers, which are listed in Table II. Also, $K_{pc,i}$ is reduced as 15 in order to establish a stable operation of the paralleled rectifiers without harmonic controllers. This is done to prove that it is the combination of using harmonic controllers and connecting rectifiers in parallel that make the system unstable and neither of the two conditions alone.

Fig. 10 shows the frequency response of the open-loop gain with multiple harmonic resonant controllers. It is clear that the rectifiers exhibit a stable terminal behavior at the PCC, which implies that the control loops of rectifiers has no effect on the instability of the minor-loop gain $T_{m,i}$. Fig. 11 compares the Nyquist plots of minor-loop gains derived with and without the harmonic resonant controllers in the paralleled operation

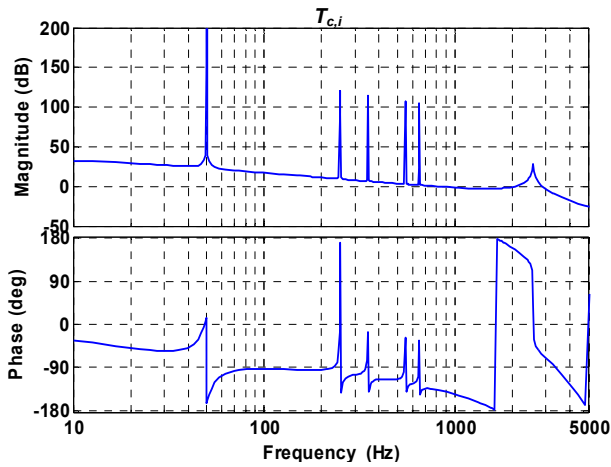


Fig. 10. Frequency response for the open-loop gain of the current control loop with the multiple harmonic resonant controllers in the i -th rectifier.

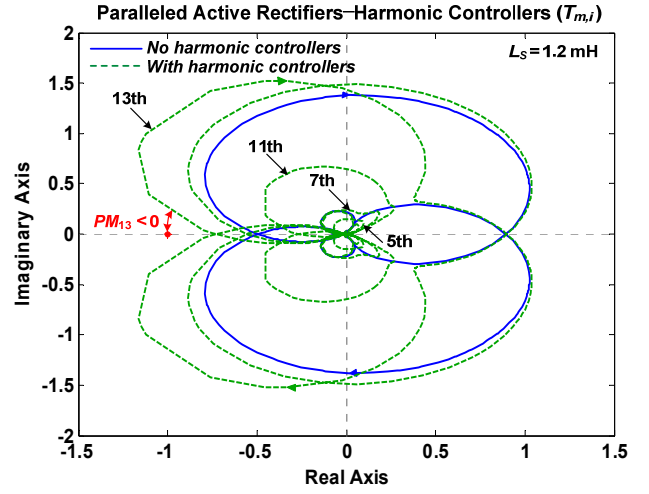
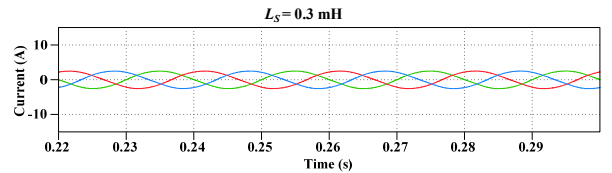


Fig. 11. Nyquist plots of the minor-loop gains derived with the multiple harmonic resonant controllers.

of rectifiers. It can be observed that for the case without the harmonic controllers, the unstable case in Fig. 8 is stabilized with a lower current control loop bandwidth ($K_{pc,i} = 15$). Nevertheless, after enabling the harmonic controllers, the phase margin around the 13th harmonic becomes negative due to the impedance interactions [35].

To validate the above frequency domain analysis, the time domain simulations based on the nonlinear switching models of the paralleled active rectifiers are performed in SIMULINK and PLECS Blockset. Notice that in order to prevent the divergence of simulations for an unstable power electronics based system, the stiff simulation solver ode15s is chosen [27], [28]. Thus, instead of the infinite time domain response, the steady-state oscillation with a much higher amplitude is obtained to indicate the instability phenomena.

Fig. 12 shows the simulated currents in the case of single active rectifier with the different grid inductances. It is clear that a severe resonance occurs in the case that L_S is 0.6 mH, which agrees with the Nyquist plots shown in Fig. 7. Fig. 13 shows the simulated currents for the case of paralleled active rectifiers. It is seen that the resonances arise when L_S is equal to 1.2 mH, which matches well with the Nyquist plots shown in Fig. 8. Fig. 14 depicts the current harmonic spectra in this resonant case, which further confirms the closed-loop frequency response shown in Fig. 9. Also, Fig. 15 shows the simulated currents for the case with the harmonic resonant controllers, which validates the Nyquist plots shown in Fig. 11.



(a)

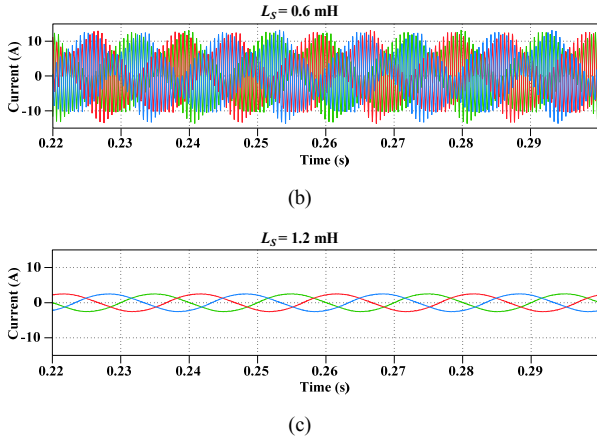


Fig. 12. Simulated currents in the case of single active rectifier under the different grid inductances. (a) $L_S = 0.3$ mH. (b) $L_S = 0.6$ mH. (c) $L_S = 1.2$ mH.

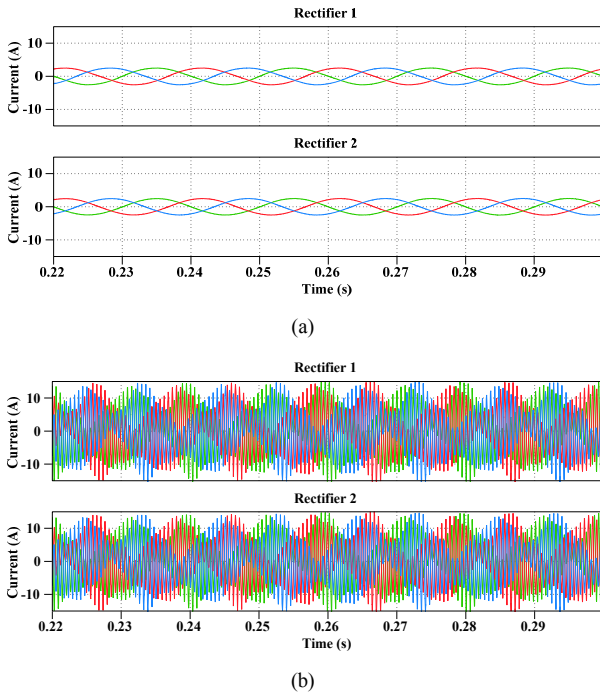


Fig. 13. Simulated currents in the case of the paralleled active rectifiers under the different grid inductances. (a) $L_S = 0.3$ mH. (b) $L_S = 1.2$ mH.

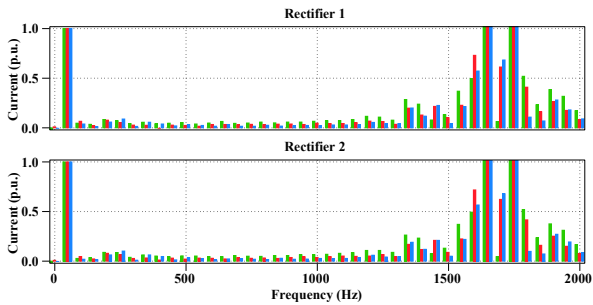


Fig. 14. Current harmonic spectra in the resonant case of paralleled active rectifiers ($L_S = 1.2$ mH, see Fig. 13).

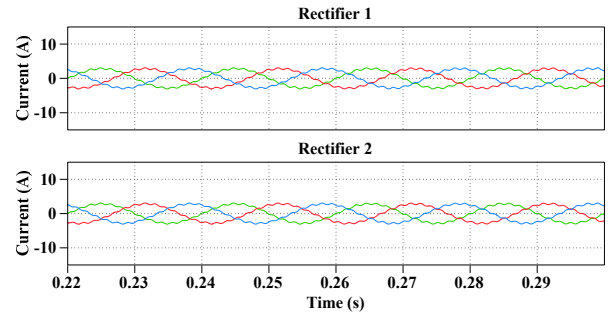


Fig. 15. Simulated currents in the case of paralleled active rectifiers with the multiple harmonic resonant controllers.

III. PROPOSED ACTIVE DAMPER

From (9), it can be found that the grid impedance Z_S results in a coupling between the paralleled active rectifiers. As in the case of an ideally stiff power grid, there are no interactions between the controllers of the paralleled active rectifiers. Thus, the basic idea behind the proposed active damper is to introduce a variable resonance damping resistance, via a power converter with a high control bandwidth, into the grid impedance profile, in order to dampen out the resonance propagation in the parallel grid-connected converters.

A. Operation Principle

Fig. 16 shows the basic configuration of the active damper used in the power electronics based AC system, which consists of a three-phase, two-level voltage source converter and a resonance damping controller. Since there is no additional energy storage element needed at the DC-link, only the active power for keeping a constant DC-link voltage is consumed by the active damper. Further, the active damper is supposed to only dampen out the resonance caused by the dynamic interactions in the parallel grid-connected converters. This is different from the conventional APFs used for the steady-state harmonic current compensation. The power rating of the active damper can thus be designed lower than the APFs, which allows a high switching frequency design. Consequently, a high control bandwidth that covers a wide range of resonance frequencies can be achieved.

Fig. 17 depicts two types of block diagrams for the resonance damping controller. The first option is similar to the R-APF method [29], as shown in Fig. 17 (a). However, instead of synthesizing the resistance at all the non-fundamental frequencies as the R-APF method, the damping resistance, $R_{d,ref}$ is only emulated at the resonance frequencies in this scheme. This is achieved by using a resonance detection block to extract the resonant voltage component, $V_{pcc,r}$ from the non-fundamental voltage, $V_{pcc,h}$. A number of signal processing techniques have been reported for harmonic estimation [30]-[32]. Among these methods, the real-time implementation of Discrete Fourier Transform (DFT) algorithm provides an attractive way to realize this resonance detection block [31].

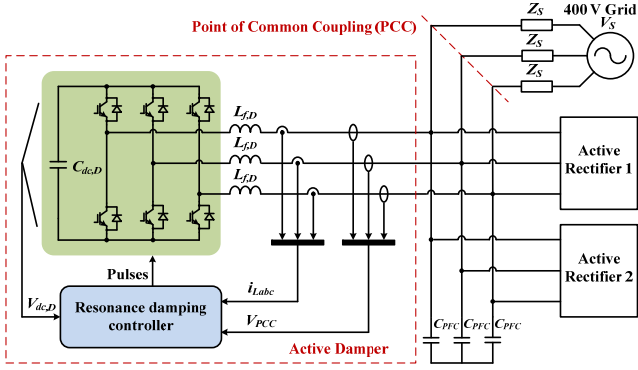
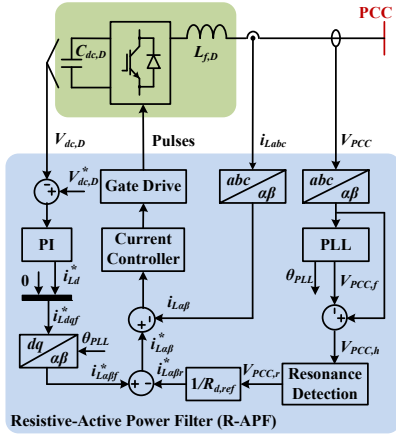
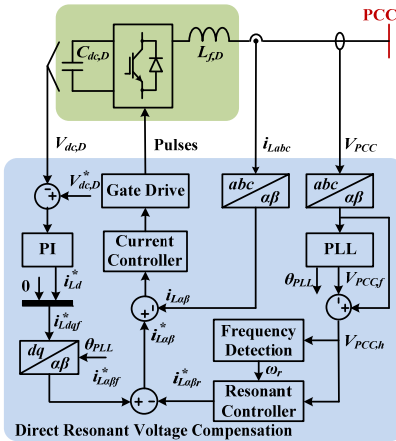


Fig. 16. Basic configuration of the proposed active damper used in the power electronics based AC system.



(a)



(b)

Fig. 17. Two types of block diagrams for the resonance damping controller. (a) R-APF method. (b) Direct resonant voltage compensation scheme.

Fig. 17 (b) illustrates the second type, where a wide-band resonant voltage controller is used to directly compensate the resonant components. This resonant voltage controller adopts the non-ideal form of resonant controller [25], [33], which is given by

$$R_{d,e} = \frac{2\omega_c s / R_{d,ref}}{s^2 + 2\omega_c s + \omega_r^2} \quad (11)$$

where $R_{d,e}$ and $R_{d,ref}$ are the actual and referenced damping resistance emulated by the active damper, respectively. ω_r and ω_c denote the resonant frequency and the bandwidth of the resonant controller, respectively. Unlike the ideal resonant controller with an infinite gain, the gain of this non-ideal resonant controller is designed as the inverse of the damping resistance, and a wide bandwidth ω_c is used to cover the adjacent resonance frequencies. Further, the resonance frequency detection block based on the DFT algorithm is employed to make the resonant controller adapted to the resonance frequency variation [31]. Thus, the resonant controller realizes both the extraction of resonant voltage component and the synthesis of damping resistance.

B. Stabilizing Effect of Active Damper

To see the stabilizing effect of the proposed active damper, the minor-loop gain is assessed considering the actual damping resistance synthesized by the active damper. Consequently, (8) and (9) are changed as

$$I_{g,i} = \frac{1}{1+T_{m,i}} G_{cl,i} I_{g,i}^* - \frac{T_{m,i}}{1+T_{m,i}} G_{cl,j} I_{g,j}^* - \frac{T_{m,i}}{1+T_{m,i}} \left(\frac{V_S}{Z_S} \right) - \frac{T_{m,i}}{1+T_{m,i}} G_{cl,d} I_{L,d}^* \quad (12)$$

$$T_{m,i} = \frac{Y_{oc,i}}{Y_{to,i}}, \quad Y_{to,i} = \frac{1}{Z_S} + Y_C + Y_{oc,j} + \frac{1}{R_{d,e}} \quad (13)$$

where $G_{cl,q}$ is the closed current control loop gain of the active damper, and $I_{L,d}^*$ is current reference of the active damper. Based on the frequency response in Fig. 9, the resonant voltage controller is designed with the center frequency at the 35th harmonic and the bandwidth of 100 Hz.

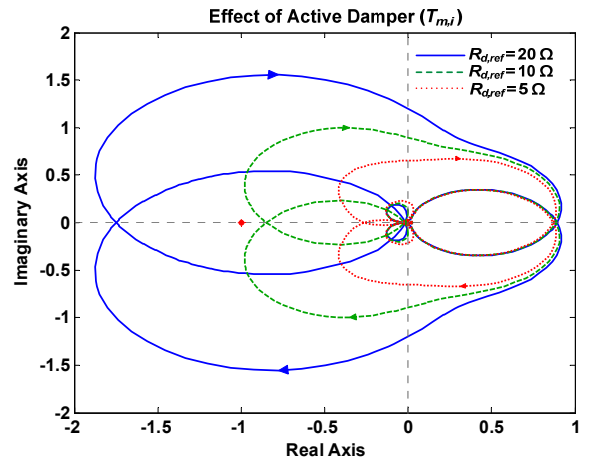


Fig. 18. Nyquist plots of the minor-loop gains with the different damping resistances of the active damper.

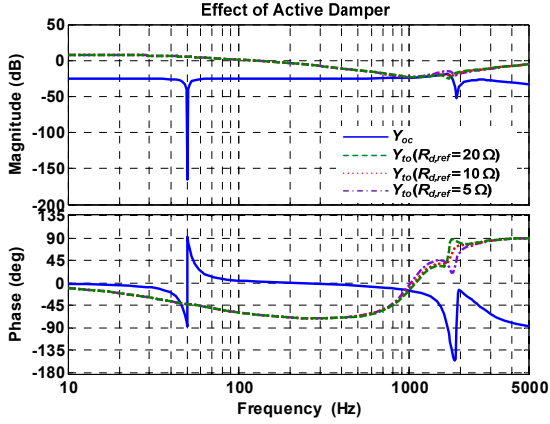


Fig. 19. Frequency responses of the input admittance of one rectifier and the total sum of the other admittances considering the active damper.

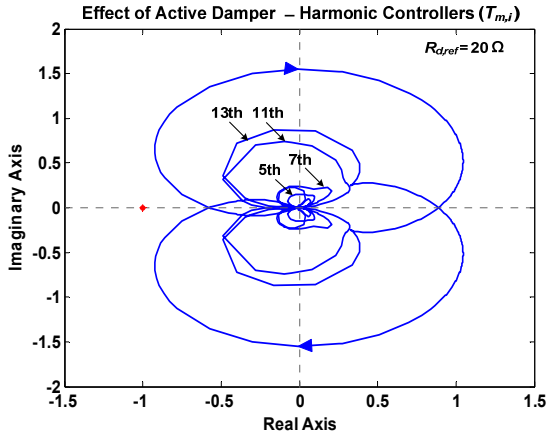


Fig. 20. Nyquist plots of the minor-loop gain derived with the multiple harmonic resonant controllers and the active damper.

Fig. 18 depicts the Nyquist plots of the minor-loop gains under the different damping resistance of the active damper. It is shown that for the resonant case of paralleled active rectifiers ($L_S = 1.2$ mH), the system becomes stabilized with the decrease of the damping resistance. Also, the frequency responses of Y_{oc} and Y_{to} are shown in Fig. 19, from which it can be seen that the intersection points between the two admittances disappear when $R_{d,ref}$ is equal to 5Ω .

Similarly, Fig. 20 depicts the stabilizing effect of the active damper for the minor-loop gains with the harmonic resonant controllers, corresponding to Fig. 11. The resonant voltage controller is designed with the center frequency at 650 Hz and the bandwidth of 50 Hz. The damping resistance is chosen as 20Ω . It is clear that the system becomes stabilized even when a large damping resistance is synthesized.

IV. SIMULATION AND EXPERIMENTAL RESULTS

To confirm the performance of the proposed active damper, the time domain simulations based on the nonlinear switching models of converters and laboratory tests are performed with a

three-converter setup. Two converters are controlled to behave as the paralleled active rectifiers shown in Fig. 1, and the last converter is controlled as the active damper. Table III gives the main parameters of the active damper.

A. Simulation Results

Corresponding to the simulated currents shown in Fig. 12 and Fig. 13, the stabilizing performances of the active damper are assessed in both the cases of single active rectifier and paralleled active rectifiers, respectively. Fig. 21 shows the simulated PCC voltage and current for the unstable case of single active rectifier ($L_S = 0.6$ mH) before and after using the active damper. The active damper is enabled at the time instant of 0.24 s. It is clear that the resonance caused by the grid impedance variation is damped by the active damper.

Fig. 22 shows the simulated currents for the resonant case of the paralleled active rectifiers ($L_S = 1.2$ mH) after applying the active damper. Compared to Fig. 13, it is seen that the instability caused by the dynamic interactions between the control loops of the paralleled active rectifiers is stabilized by the active damper. Fig. 23 shows the changes of the PCC voltage once the active damper is enabled at the instant of 0.24 s. An effective resonance damping on the PCC voltage can be observed.

Fig. 24 shows the output current of the active damper and the associated harmonic spectra in the case of paralleled active rectifiers. It is seen that the fundamental frequency current is

TABLE III. MAIN PARAMETERS OF ACTIVE DAMPER

Parameters		Values
Filter inductance	$L_{f,D}$	3 mH
DC capacitor	$C_{dc,D}$	660 μ F
Switching frequency	f_{sw}	20 kHz
Sampling period	T_S	50 μ s
DC-link voltage	$V_{dc,D}$	700 V
PR current controller	$K_{p,i}$	30
	$K_{r,i}$	600
DC-link voltage controller	$K_{p,dc,D}$	0.05
	$K_{i,dc,D}$	0.5
Resonant controller	$K_{r,v}$	2
	ω_r	3500π rad/s

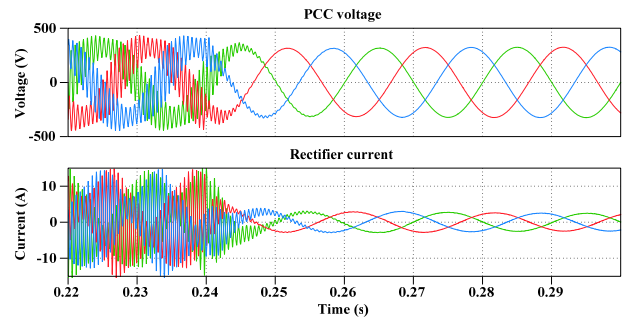


Fig. 21. Simulated PCC voltage and current for the unstable case of single active rectifier ($L_S = 0.6$ mH) before and after using the active damper at 0.24 s.

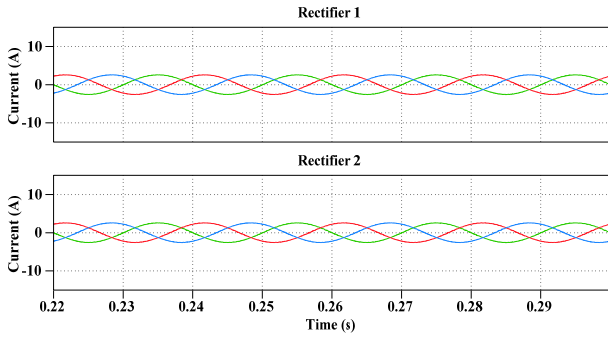


Fig. 22. Simulated currents for the unstable case of paralleled active rectifiers ($L_S=1.2$ mH) after using the active damper.

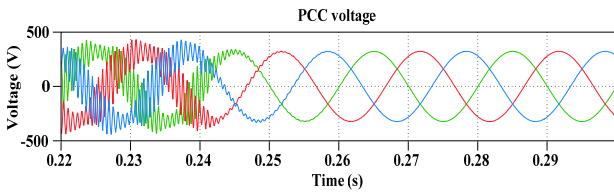


Fig. 23. Simulated PCC voltage in the unstable case of paralleled active rectifiers ($L_S=1.2$ mH) before and after applying the active damper at 0.24 s.

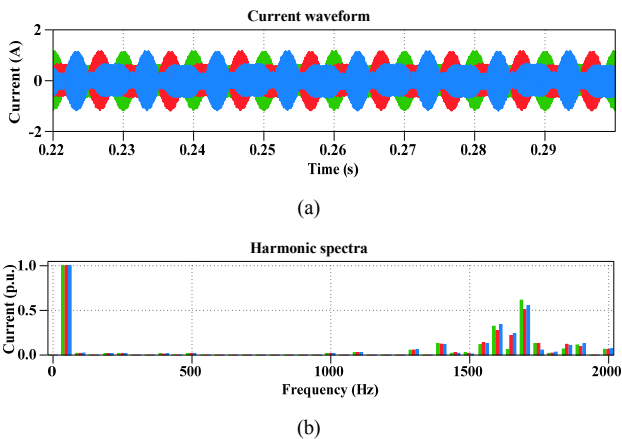


Fig. 24. Simulated current of the active damper and the associated harmonic spectra. (a) Current waveform. (b) Harmonic spectra.

low due to the absence of the additional energy storage element in the DC side, whereas the resonant frequencies currents are relative larger compared to the fundamental frequency current. This implies that the active damper has to absorb a certain amount of resonance currents for stabilizing the paralleled converters.

B. Experimental Results

Fig. 25 shows the hardware picture of the built laboratory test setup, where three parallel grid-connected Danfoss frequency converters are used as the two paralleled active rectifiers and the active damper. The control algorithms for the converters are implemented in DS1006 dSPACE system.

Considering the grid background harmonic voltages and the

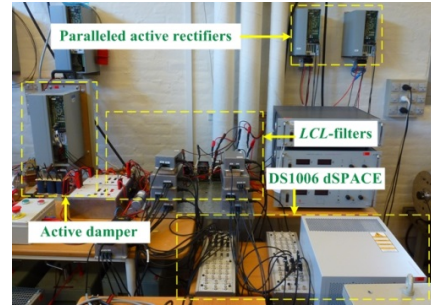


Fig. 25. Hardware picture of the built laboratory setup.

low-order harmonics caused by the dead time, the multiple harmonic resonant controllers (5th, 7th, 11th and 13th) are enabled in the laboratory tests. Further, owing to the nonlinear behavior of the filter inductor and the parameter drift at high frequencies, only the effect of the impedance interactions on the minor-loop gains derived with the multiple harmonic resonant controllers is considered in the laboratory tests.

Fig. 26 shows the measured output currents and for the paralleled active rectifiers before applying the active damper. The measured PCC voltage waveform in this case is shown in Fig. 27. It can be seen that a low-order harmonic resonance propagates in the test setup. To further identify the resonance frequency, Fig. 28 shows the harmonic spectra of the PCC voltage. It is clear that the harmonic resonance arises at the 13th harmonic, which agrees well with the frequency domain

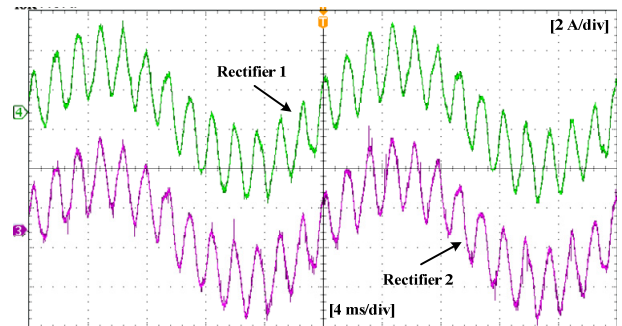


Fig. 26. Measured output currents of the paralleled active rectifiers before applying the active damper (2 A/div, 4 ms/div).

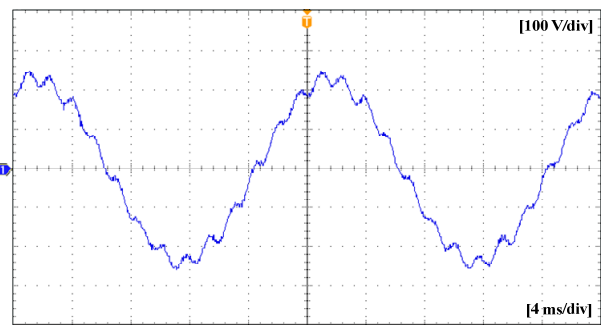


Fig. 27. Measured PCC voltage waveform before applying the active damper (100 V/div, 4 ms/div).

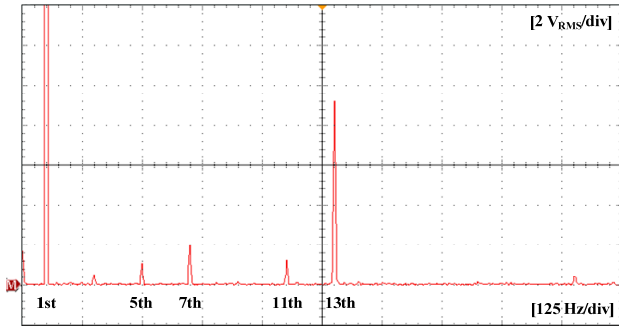


Fig. 28. Harmonic spectra of the measured PCC voltage before applying the active damper ($2 V_{RMS}/div$, $125 Hz/div$).

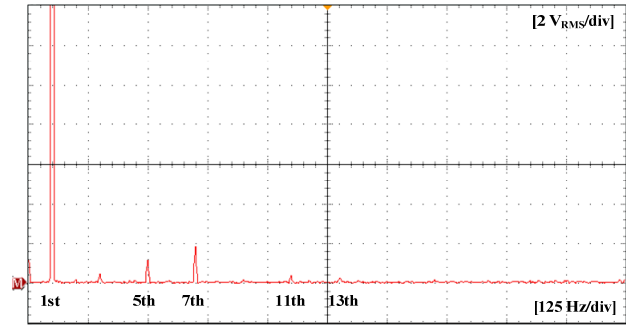


Fig. 31. Harmonic spectra of the measured PCC voltage after applying the active damper ($2 V_{RMS}/div$, $125 Hz/div$).

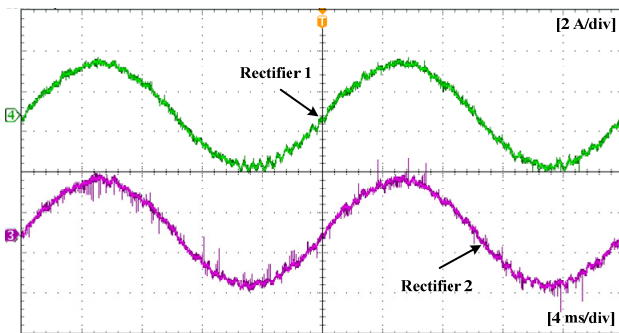


Fig. 29. Measured output currents of the paralleled active rectifiers after applying the active damper ($2 A/div$, $4 ms/div$).

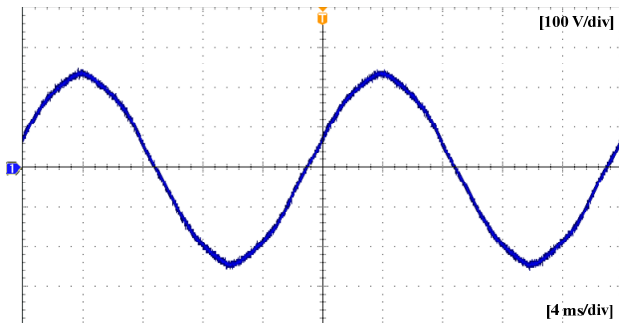


Fig. 30. Measured PCC voltage waveform after applying the active damper ($100 V/div$, $4 ms/div$).

analysis shown in Fig. 11 and time domain simulation result shown in Fig. 15.

In contrast, Fig. 29 shows the measured output currents of the paralleled active rectifiers after enabling the active damper. It is evident that the thirteenth harmonic resonance is effectively damped, and also the low-order harmonic currents caused by the background harmonics are compensated by the harmonic resonant controllers. Fig. 30 shows the measured PCC voltage waveform with the use of active damper and its harmonic spectra is shown in Fig. 31. It is seen that the harmonic resonance propagation in the system is damped by the active damper, which matches with the frequency domain analysis in Fig. 20.

V. CONCLUSIONS

This paper has discussed the resonance propagation in the parallel grid-connected converters. An active damper concept for stabilizing such a power electronics based AC systems has been proposed. Although several active stabilization schemes have been reported in the previous work, most of them are embedded in the control systems of the converters. As a consequence, the performances of those approaches are either limited by the characteristics of converters or sensitive to the system conditions, which tend to cause the additional resonances. In contrast, the proposed active damper aims to provide a versatile device that can be plug-and-play under the different applications. Further, the active damper only takes effect on the resonance damping, which allows a lower power and higher control bandwidth compared to the conventional APFs. Two control topologies of the active damper have been discussed. Note that the direct resonant voltage compensation method simplifies the synthesis of the variable resistance at the resonance frequencies compared to the R-APF approach. Finally, the time domain simulations on the nonlinear switching models of converters and the experimental tests have been carried out. The results have confirmed the stabilizing performance of the proposed active damper.

REFERENCES

- [1] F. Blaabjerg, Z. Chen, and S. B. Kjaer, "Power electronics as efficient interface in dispersed power generation systems," *IEEE Trans. Power Electron.*, vol. 19, no. 5, pp. 1184-1194, Sep. 2004.
- [2] J. Rocabert, A. Luna, F. Blaabjerg, and P. Rodriguez, "Control of power converters in AC microgrids," *IEEE Trans. Power Electron.*, vol. 27, no. 11, pp. 4734-4749, Nov. 2012.
- [3] P. Brogan, "The stability of multiple, high power, active front end voltage sourced converters when connected to wind farm collector system," in *Proc. EPE Wind Energy Chapter Seminar 2010*, pp. 1-6.
- [4] J. Agorreta, M. Borrega, J. Lopez, and L. Marroyo, "Modeling and control of N -paralleled grid-connected inverters with LCL filter coupled due to grid impedance in PV plants," *IEEE Trans. Power Electron.*, vol. 26, no. 3, pp. 770-785, Mar. 2011.
- [5] E. Mollerstedt and B. Bernhardsson, "Out of control because of harmonics—An analysis of the harmonic response of an inverter locomotive," *IEEE Control Syst. Mag.*, vol. 20, no. 4, pp. 70-81, Aug. 2000.
- [6] R. Turner, S. Walton, and R. Duke, "Stability and bandwidth implications of digitally controlled grid-connected parallel inverters," *IEEE Trans. Ind. Electron.*, vol. 57, no. 11, pp. 3685-3694, Nov. 2010.

- [7] X. Wang, F. Blaabjerg, and Z. Chen, "Autonomous control of inverter-interfaced distributed generation units for harmonic current filtering and resonance damping in an islanded microgrid," *IEEE Trans. Ind. Appl.*, Early Access Article, 2013.
- [8] F. Wang, J. L. Duarte, M. A. M. Hendrix, and P. F. Ribeiro, "Modeling and analysis of grid harmonic distortion impact of aggregated DG inverters," *IEEE Trans. Power Electron.*, vol. 26, no. 3, pp. 786-797, Mar. 2011.
- [9] J. Sun, "Small-signal methods for AC distributed power systems—a review," *IEEE Trans. Power Electron.*, vol. 24, no. 11, pp. 2545-2554, Nov., 2009.
- [10] R. D. Middlebrook, V. Vorperian, and L. Lindal, "The N extra element theorem," *IEEE Trans. Circuits Syst. I: Fundam. Theory Appl.*, vol. 45, no. 9, pp. 919-935, Sep. 1998.
- [11] L. Harnefors, M. Bongiorno, and S. Lundberg, "Input-admittance calculation and shaping for controlled voltage-source converters," *IEEE Trans. Ind. Electron.*, vol. 54, no. 6, pp. 3323-3334, Dec. 2007.
- [12] L. Harnefors, L. Zhang, and M. Bongiorno, "Frequency-domain passivity-based current controller design," *IET Power Electron.*, vol. 1, no. 4, pp. 455-465, Dec. 2008.
- [13] L. Harnefors, "Analysis of subsynchronous torsional interaction with power electronic converters," *IEEE Trans. Power Syst.*, vol. 22, no. 1, pp. 305-313, Feb. 2007.
- [14] J. He, Y. W. Li, D. Bosnjak, and B. Harris, "Investigation and active damping of multiple resonances in a parallel-inverter-based microgrid," *IEEE Trans. Power Electron.*, vol. 28, no. 1, pp. 234-246, Jan. 2013.
- [15] X. Wang, F. Blaabjerg, and Z. Chen, "Synthesis of variable harmonic impedance in inverter-interfaced distributed generation unit for harmonic damping throughout a distribution network," *IEEE Trans. Ind. Appl.*, vol. 48, no. 4, pp. 1407-1417, Jul./Aug. 2012.
- [16] L. Kocewiak, "Harmonics in large offshore wind farms," Ph.D. Dissertation, Aalborg Univ., Aalborg, Denmark, 2012.
- [17] M. Liserre, F. Blaabjerg, and S. Hansen, "Design and control of an LCL-filter-based three-phase active rectifier," *IEEE Trans. Ind. Appl.*, vol. 41, no. 5, pp. 1281-1291, Sep./Oct. 2005.
- [18] R. Turner, S. Walton, and R. Duke, "A case study on the application of the Nyquist stability criterion as applied to interconnected loads and sources on grids," *IEEE Trans. Ind. Electron.*, vol. 60, no. 7, pp. 2740-2749, Jul. 2013.
- [19] M. Liserre, R. Teodorescu, and F. Blaabjerg, "Stability of photovoltaic and wind turbine grid-connected inverters for a large set of grid impedance values," *IEEE Trans. Power Electron.*, vol. 21, no. 1, pp. 263-272, Jan. 2006.
- [20] B. Wen, D. Boroyevich, P. Mattavelli, Z. Shen, and R. Burgos, "Experimental verification of the generalized Nyquist stability criterion for balanced three-phase AC systems in the presence of constant power loads," in *Proc. IEEE ECCE 2012*, pp. 3926-3933.
- [21] M. Corradini, P. Mattavelli, M. Corradin, and F. Polo, "Analysis of parallel operation of uninterruptible power supplies loaded through long wiring cables," *IEEE Trans. Power Electron.*, vol. 25, no. 4, pp. 1046-1054, Apr. 2010.
- [22] S. Vesti, T. Suntio, J. A. Oliver, R. Prieto, and J. A. Cobos, "Impedance-based stability and transient-performance assessment applying maximum peak criteria," *IEEE Trans. Power Electron.*, vol. 28, no. 5, pp. 2099-2104, May 2013.
- [23] J. Sun, "Impedance-based stability criterion for grid-connected converters," *IEEE Trans. Power Electron.*, vol. 26, no. 11, pp. 3075-3078, Nov. 2011.
- [24] J. Yin, S. Duan, and B. Liu, "Stability analysis of grid-connected inverter with LCL filter adopting a digital single-loop controller with inherent damping characteristic" *IEEE Trans. Ind. Inform.*, vol. 9, no. 2, pp. 1104-1112, May 2013.
- [25] D. N. Zmood and D. G. Holmes, "Stationary frame current regulation of PWM inverters with zero steady-state error," *IEEE Trans. Power Electron.*, vol. 18, no. 3, pp. 814-822, May 2003.
- [26] V. Blasko and V. Kaura, "A new mathematical model and control of a three-phase AC-DC voltage source converter," *IEEE Trans. Power Electron.*, vol. 12, no. 1, pp. 116-123, Jan. 1997.
- [27] PLECS Blockset – The power electronics toolbox for Simulink, Plexim GmbH, Zurich, Switzerland, [Online]. Available: <http://www.plexim.com/>.
- [28] *Simulink User's Guide*, MathWorks, Natick, MA.
- [29] H. Akagi, H. Fujita, and K. Wada, "A shunt active filter based on voltage detection for harmonic termination of a radial power distribution line," *IEEE Trans. Ind. Appl.*, vol. 35, no. 3, pp. 638-645, May/June 1999.
- [30] L. Asiminoaei, F. Blaabjerg, and S. Hansen, "Detection is key – harmonic detection methods for active power filter applications," *IEEE Ind. Appl. Mag.*, vol. 13, no. 4, pp. 22-33, Jul./Aug. 2007.
- [31] E. Lavopa, P. Zanchetta, M. Sumner, and F. Cupertino, "Real-time estimation of fundamental frequency and harmonics for active shunt power filters in aircraft electrical systems," *IEEE Trans. Ind. Electron.*, vol. 56, no. 8, pp. 2875-2884, Aug. 2009.
- [32] X. Zhou, J. Fan, and A. Q. Huang, "High-frequency resonance mitigation for plug-in hybrid electric vehicles' integration with a wide range of grid conditions," *IEEE Trans. Power Electron.*, vol. 27, no. 11, pp. 4459-4471, Nov. 2012.
- [33] R. Teodorescu, F. Blaabjerg, M. Liserre, and P. C. Loh, "Proportional-resonant controllers and filters for grid-connected voltage-source converters," *IEE Proc.-Electr. Power Appl.* vol. 153, no. 5, pp. 750-762, Sep. 2006.
- [34] A. G. Yepes, F. D. Freijedo, O. Lopez, and J. D. Gandoy, "High-performance digital resonant controllers implemented with two integrators," *IEEE Trans. Power Electron.*, vol. 26, no. 2, pp. 563-576, Feb. 2011.
- [35] A. G. Yepes, F. D. Freijedo, O. Lopez, and J. D. Gandoy, "Analysis and design of resonant current controllers for voltage-source converters by means of Nyquist diagrams and sensitive function," *IEEE Trans. Ind. Electron.*, vol. 58, no. 11, pp. 5231-5250, Nov. 2011.